Science Journal of Chemistry
2021; 9(4): 80-96
http://www.sciencepublishinggroup.com/j/sjc
doi: 10.11648/j.sjc.20210904.11
ISSN: 2330-0981 (Print); ISSN: 2330-099X (Online)

Electric Field Effects on Neutral Gold Clusters Au_{2-10}: A First-Principles Theoretical Survey of the First- and Second-Order Hyperpolarizabilities

Mahnaz Jabbarzadeh Sani

Chemistry Department, College of Science, Shiraz University, Shiraz, Iran

Email address:
mjsani@shirazu.ac.ir

To cite this article:
Mahnaz Jabbarzadeh Sani. Electric Field Effects on Neutral Gold Clusters Au_{2-10}: A First-Principles Theoretical Survey of the First- and Second-Order Hyperpolarizabilities. *Science Journal of Chemistry*. Vol. 9, No. 4, 2021, pp. 80-96. doi: 10.11648/j.sjc.20210904.11

Received: June 28, 2021; **Accepted**: July 19, 2021; **Published**: July 29, 2021

Abstract: Herein we report the density functional theory (DFT) calculations of nonlinear optical (NLO) properties of neutral gold clusters Au_n (n=2-10) applying long-range corrected LC-M06L functional and Los-Alamos National Laboratory double-ζ polarized basis set. The effects of the incident frequency on the first and second-order hyperpolarizability together with the influence of the external electric field on the frontier orbitals of neutral gold clusters are investigated. It is found that the application of external electric field can increase or decrease the gap energy of neutral gold clusters depending on the direction and magnitude of the applied field. More importantly, by correctly controlling the direction and magnitude of the external electric field, reactive gold clusters having low gap energies can be achieved. Furthermore, the external electric field has more important effect on the virtual orbitals of gold hexamer and decreases the energy of these orbitals along the directions parallel to the molecular plane, resulting in low-energy excitations. The low-energy excitations are expected to play important role in the high second-order hyperpolarizability and better response to the applied field. The third-order nonlinear (NLO) properties of gold hexamer are also strongly affected by the frequency of the incident light and thus can be tuned using the incident frequency for applications. The present work may propose new strategies for enhancing the nonlinear optical response of neutral gold clusters.

Keywords: Nonlinear Optics, Gold Cluster, Electric Field, Density Functional Theory

1. Introduction

Metal clusters are formed by assembling a small number of atoms ranging from a few to several hundred [1]. Among them, gold nanoparticles have received great interest in electronics [2, 3], catalysis [4, 5], chemical sensing [6], optical limiting [7, 8], optics [9] and biomedical fields [10-15]. The field of optics investigates the interaction between matter and light resulting in specific optical properties of individual material which are essentially determined by the response of the electrons to an external electric field [16]. Due to discrete energy levels and molecular-like HOMO-LUMO transitions, ultrasmall clusters exhibit a spectacular optical behavior which is fundamentally different from that of larger plasmonic nanocrystals [17]. It has been established that transition to the plasmonic regime sets in progressively with size, and at 144 atoms (Au_{144}) weak absorption saturation manifests in the z-scan curve [18]. The investigation of static first hyperpolarizabilities of eight model clusters $[Au_m(SH)_n]^z$ (m=18-38) by means of density functional theory revealed that no correlation between cluster size and static first hyperpolarizability can be identified [19]. Instead, the symmetry of the clusters seems to dominate the nonlinear optics (NLO) properties. For instance, at a fundamental wavelength of 800 nm, the $Au_{38}(SCH_2CH_2Ph)_{24}$ cluster is active, while $Au_{25}(SCH_2CH_2Ph)_{18}$ does not yield significant second-harmonic generation (SHG) signal due to center of inversion in the Au_{25} cluster [20]. By experimentally probing thickness-dependent changes of band structure using two-photon photoluminescence, a surprisingly 100-fold increase of the nonlinear signal was observed when the gold film thickness was reduced bellow 30 nm [21].

Furthermore, the first hyperpolarizability β for Au_{15} cluster (509×10^{-30} esu) as compared to Au_{25} cluster (128×10^{-30} esu) is larger considering the difference in the number of gold atoms [17]. The 10^{30} β per atom values reported for Au_{15} and Au_{25} clusters are more than two-orders of magnitude larger than the values reported for AuNPs in the size range 10-50 nm. The $Au_{10}(SG)_{10}$ cluster also presents a large first hyperpolarizability [22]. In addition, the first-hyperpolarizability $\beta(-2\omega;\omega,\omega)$ of gold nanocluster $Au_6(GSH)_2(MPA)_2$ having six gold atoms is in comparison with larger AuNCs, the largest value ever reported [23]. Hence, by considering non-linear optical properties of gold quantum clusters, it has been revealed that the smaller gold clusters are better due to providing larger first hyperpolarizabilities [17, 22, 23].

Recent efforts have been done on the nonlinear optical (NLO) properties determination of metal clusters with the number of metal atoms higher than 10 [16-33], while the only reported nonlinear optical properties of gold cluster with a number of metal atoms lower than 10 has been for the gold nanocluster $Au_6(GSH)_2(MPA)_2$ having six gold atoms [23]. We herein present density functional theory (DFT) calculations of the nonlinear optical (NLO) properties of gas-phase gold clusters Au_n (n=2-10) as a first approach towards the theoretical exploration of their NLO properties. The influence of the external electric field on the frontier molecular orbital (HOMO-LUMO) gap energies of gold clusters is also discussed. We assess the effects of incident frequency on the first- and second-order hyperpolarizability. Our study may propose new strategies for enhancing the nonlinear optical (NLO) responses of neutral gold nanoclusters Au_n (n=2-10) by modulating the frequency of incident light.

2. Computational Details

For geometry optimizations, the coordinates of neutral gold clusters Au_n (n=3-8) were selected based on the available experimentally-theoretically determined structures in the literature [34-36]. To obtain global minima of Au_9 and Au_{10} clusters, a series of structures were built based on our designed or previously reported geometries [35-40], and optimized using the B3LYP functional in combination with the Los-Alamos National Laboratory double-ζ polarized basis set for gold. Hay and Wadt [41-43] have proposed these relativistic effective core potentials to enable valence electron calculations to be carried out with essentially the same accuracy as all electron calculations, but with much less computational effort. The LANL2DZ basis set incorporates the mass-velocity and Darwin relativistic effects into the potential and explicitly deals with 19-valence electrons per Au atom through a split valence double-ζ basis set [44]. The calculations were performed in the spin states, singlet, doublet, triplet, quartet, quintet and sextet. Harmonic vibrational analyses were performed in order to discriminate between minima and possible transition states on the potential energy surface. Then, depending on the energy distribution of the cluster isomers, the most stable one to three isomers for each cluster size were further optimized using the LC-M06L functional and Los-Alamos National Laboratory double-ζ polarized basis set for gold. A final vibrational analysis was also carried out.

In order to determine the best functional to be used for the calculations, we made a comparative study of the vibrational frequency, ionization potential and bond length of the gold dimer as well as the mean static polarizability of atomic gold. The results are compared with the available experimentally determined values in Table 1.

Table 1. *Vibrational frequency (ω_e/Cm^{-1}), ionization potential (IP/eV) and bond length (R_e/A°) of gold dimer together with the mean static polarizability (<α>/A^{o3}) of atomic gold.*

Method	Au_2			Au
	IP/eV	ω_e/Cm^{-1}	R_e/A°	<α>/A^{o3}
CAM-B3LYP	9.30	174	2.547	5.65
B3LYP	9.49	162	2.573	5.45
B1LYP	9.27	161	2.579	5.49
X3LYP	9.44	163	2.572	5.45
PBEPBE	9.58	168	2.551	5.42
PBE1PBE	9.33	173	2.543	5.67
mPW1PW91	9.34	172	2.543	5.71
PW91PW91	9.64	169	2.548	5.43
B3PW91	9.43	171	2.547	5.65
B1B95	9.26	173	2.542	5.60
mPW3PBE	9.46	172	2.542	5.62
B3P86	10.1	173	2.540	5.58
mPW1LYP	9.31	162	2.578	5.46
mPW1PBE	9.33	173	2.540	5.71
B98	9.41	165	2.563	5.60
B971	9.36	164	2.568	5.58
B972	9.32	166	2.554	5.71
PBEh1PBE	9.35	171	2.549	5.70
BHandHLYP	8.98	166	2.571	5.73
BMK	9.36	176	2.583	5.29
HSEh1PBE	9.37	170	2.550	5.68
WB97	8.98	175	2.553	5.97
WB97x	9.08	174	2.556	5.93
TPSS	9.45	174	2.537	5.65
TPSSh	9.37	175	2.537	5.73
VSXC	9.53	161	2.572	5.21
M06	9.14	158	2.592	5.90
M06L	9.04	162	2.557	5.57
M06HF	11.1	191	2.522	6.62
M06-2x	8.83	161	2.586	5.16
HCTH	9.63	153	2.572	5.51
HCTH93	9.41	155	2.569	5.52
HCTH147	9.66	158	2.563	5.43
tHCTH	9.67	168	2.539	5.97
tHCTHhyb	9.67	166	2.548	5.64
LC-tHCTH	9.76	173	2.556	5.63
LC-HCTH147	9.48	176	2.545	5.80
LC-HCTH407	9.36	166	2.568	5.74
LC-HCTH93	9.23	173	2.548	5.87
LC-M06L	9.49	183	2.520	5.77
Exp.	9.50[a]	191[a]	2.472[b]	5.79±1.45[c]

a, b and c indicate Refs. [36], [40] and [45], respectively.

Among the functionals used, The M06HF functional gives

the best value of vibrational frequency, but the ionization potential is overestimated. The bond length calculated by the M06-2x, BMK, B1LYP, mPW1LYP and B3LYP functionals is far too high. The HCTH, HCTH93, HCTH147, LC-HCTH147, LC-HCTH407, LC-HCTH93, tHCTHLyb, BHandHLyb, tHCTH, LC-tHCTH, mPW1PW91, PBEPBE, PBE1PBE, PW91PW91, mPW1LYP, mPW3PBE, mPW1PBE, HSEh1PBE, PBEh1PBE, B3PW91, B98, B971, B972, BMK, WB97, WB97x, B1B95, B3P86, B1LYP, B3LYP, X3LYP, CAM-B3LYP, TPSS, TPSSh, VSXC, M06, M06-2x and M06L functionals underestimate the vibrational frequency. Among all the available functionals, it is clear that the LC-M06L functional results in the best values for all the parameters considered. Hence, we choose this functional for the present computations. The LC-M06L functional contains a long-range correction scheme for generalized-gradient approximation exchange functionals. This long-range correction scheme employs the local density approximation for the short-range part and the Hartree-Fock exchange integral for the long-range part [46].

The response of an atom or molecule to applied field F can be approximated as [47-49],

$$\mu_i = \langle \Psi(F,t)|\hat{\mu}_i|\Psi(F,t)\rangle = \mu_{0i} + \alpha_{ij}F_j + \frac{1}{2!}\beta_{ijk}F_jF_k + \frac{1}{3!}\gamma_{ijkl}F_jF_kF_l + \ldots \quad (1)$$

where the subscripts "i, j, etc." relate to the Cartesian coordinates in atomic or molecular axes on which the external field is projected. μ is the dipole moment vector and α, β and γ are polarizability, first- and second-order hyperpolarizability tensors of ranks two, three and four, respectively. For centrosymmetric molecules, the β tensor and all odd rank tensors vanish due to symmetry [48]. When a time-dependent electric field $F = F_0 + F_\omega \cos(\omega t)$ is applied, the expansion (1) can be rewritten as [47, 49],

$$\mu_i = \mu_{0i} + \alpha_{ij}(0;0)F_j + \alpha_{ij}(-\omega;\omega)F_{\omega j}\cos(\omega t) + \frac{1}{2}\beta_{ijk}(0;0,0)F_{0j}F_{0k} + \beta_{ijk}(-\omega;\omega,0)F_{\omega j}F_{0k}\cos(\omega t)$$
$$+ \frac{1}{4}\beta_{ijk}(-2\omega;\omega,\omega)F_{\omega j}F_{\omega k}\cos(2\omega t) + \frac{1}{6}\gamma_{ijkl}(0;0,0,0)F_{0j}F_{0k}F_{0l} + \frac{1}{2}\gamma_{ijkl}(-\omega;\omega,0,0)F_{\omega j}F_{0k}F_{0l}\cos(\omega t)$$
$$+ \frac{1}{8}\gamma_{ijkl}(-\omega;\omega,-\omega,\omega)F_{\omega j}F_{\omega k}F_{\omega l}\cos(\omega t) + \frac{1}{4}\gamma_{ijkl}(-2\omega;\omega,\omega,0)F_{\omega j}F_{\omega k}F_{0l}\cos(2\omega t) + \ldots \quad (2)$$

where, the first- and second-order hyperpolarizability coefficients are defined as: β(0;0,0) for static first-order hyperpolarizability, β(-2ω ;ω ,ω) for second-harmonic generation, γ(0;0,0,0) for static second-order hyperpolarizability, γ(-ω ;ω ,0,0) for optical Kerr effect (OKE), γ(-ω ;ω ,-ω ,ω) for degenerate four-wave mixing (DFWM) and γ(-2ω ;ω ,ω ,0) for electric-field-induced second harmonic generation (EFISHG). We use the following relation to calculate the degenerate four-wave mixing (DFWM) second-order hyperpolarizability coefficient [49]

$$\gamma(-\omega;\omega,-\omega,\omega) = \frac{1}{3}\gamma(-2\omega;\omega,\omega,0) + \gamma(-\omega;\omega,0,0) - \frac{1}{3}\gamma(0;0,0,0) \quad (3)$$

The static and second-harmonic generation mean first-order hyperpolarizability coefficients are defined as [50],

$$\beta(0;0,0) = (\beta_x^2 + \beta_y^2 + \beta_z^2)^{1/2};$$

$$\beta_i = \frac{3}{5}(\beta_{iii} + \beta_{ijj} + \beta_{ikk}) \quad (4)$$

$$\beta(-2\omega;\omega,\omega) = (\beta_x^2 + \beta_y^2 + \beta_z^2)^{1/2};$$

$$\beta_i = \frac{1}{5}(\beta_{ijj} + 2\beta_{jji} + \beta_{ikk} + 2\beta_{kki} + 3\beta_{iii}) \quad (5)$$

where the subscripts "i,j,k" relate to the Cartesian coordinates x, y, and z. The mean second-order hyperpolarizability is calculated using the following relation [49],

$$\gamma = \frac{1}{15}\sum_{\xi\eta}(\gamma_{\xi\xi\eta\eta} + \gamma_{\xi\eta\eta\xi} + \gamma_{\xi\eta\xi\eta});\ \xi, \eta = x, y, z. \quad (6)$$

All computations were performed using Gaussian 09 program package [51]. The geometries were visualized applying GaussView software [52] and the density of states were calculated using the GaussSum 3.0 program [53]. The Natural population analyses were performed Using NBO under Gaussian 09 program package [54].

3. Results and Discussion

3.1. Geometric and Electronic Characteristics

Results obtained for the neutral gold clusters $Au_{2\text{-}10}$ are summarized in Table 2, where their global minima structures, bond lengths, symmetries and electronic states are listed. As can be seen in this Table, planar structures are found to represent the putative global minima. The two-dimensional (2D) structures have been reported in previous studies as the most stable isomers, thus confirming that our method works well [34-36, 38]. The main purpose is to examine the effect of an external electric field on the response of gold clusters to the applied field; however, before we proceed to compute the optical responses for neutral gold clusters, it is important to see the influence of electric field on the HOMO-LUMO gap energies of these clusters.

3.1.1. The Effect of External Electric Field on the Electronic Characteristics of Gold Dimer

To better understand, we first present comprehensive study of the influence of an external electric field on the electronic characteristics of the gold dimer.

Table 2. *Global minima, bond distances, symmetries and electronic states of Au_{2-10} clusters.*

Structure	Shape	Bond distance (A°)	Symmetry	Electronic state
	Linear	2.520	$D_{\infty h}$	$^1\Sigma_g$
	Triangle	2.618-2.860	C_{2v}	$^2B_2$
	Rhombus	2.620-2.693	C_{2v}	$^1A_1$
	W-form	2.643-2.752	C_{2v}	$^2A_1$
	Triangle	2.647-2.784	D_{3h}	$^1A_1'$
	Capped triangle	2.641-2.877	Cs	$^2A'$
	Tetra-capped rhombus	2.630-2.756	Cs	$^1A'$
	Bi-capped hexagon	2.642-2.953	C_{2v}	$^2A_1$
	Tri-capped hexagon	2.694-2.774	D_{2h}	^1A_g

Figure 1 illustrates the behavior of the highest occupied-lowest unoccupied (HOMO-LUMO) molecular orbitals of gold dimer in the presence of an external electric field along the axial direction of the linear Au_2 molecule.

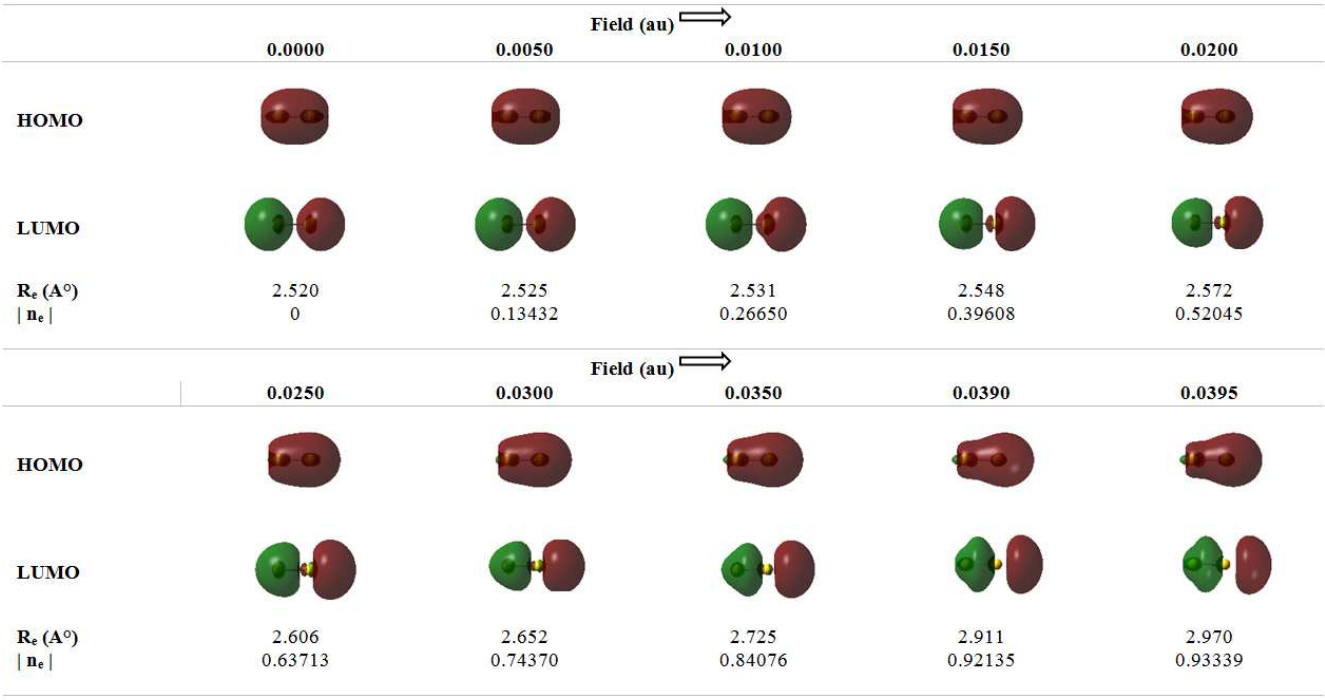

Figure 1. *HOMO-LUMO molecular orbitals, bond lengths (R_e/A°) and natural charges ($|n_e|$) of Au_2 molecule in the absence and presence of external electric field.*

As this Figure shows, the Au-Au distance increases from 2.520 to 2.970 A°, as the electric field increases from 0 to 0.0395 au (0.001 au = 0.05142 V/A° [55]). The ionization of gold dimer occurs at the electric field value of 0.0396 au. Figure 1 also represents the effect of the static external electric field on the frontier orbitals (HOMO-LUMO) of gold dimer. It is clear that the application of external electric field along the axial direction of Au_2 molecule breaks the orbital symmetry of the frontier orbitals. The breaking of orbital symmetry of HOMO and LUMO is due to the polarization of gold dimer in the presence of external electric field. As in the Gaussian program package, the direction of electric field vector is from minus to plus [56] (Figure 2), the external electric field pushes the lobes of HOMO and LUMO from

left to right (Figure 1). This is beneficial to the enhancement of charge transfer along the direction of electric field.

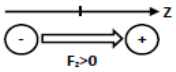

Figure 2. *A graphical depiction of the electric field convention in the Gaussian package.*

A natural population analysis (NPA) reveals that the natural charge increases from 0 to 0.93339 as the external electric field increases from 0 to 0.0395 au and at the electric field value of 0.0396 au, ionization of gold dimer occurs by transferring one electron from the left to the right gold atom. As Table 3 shows, at the external electric field value of 0.0395 au, the charge has nearly transferred from orbital "6s" located on the left atom to the orbitals "6s, 5d, 6p and 7p" located on the right gold atom. Finally, at the external electric field value of 0.0396 au gold dimer dissociates and in the presence of this field, the cationic and anionic gold atoms have the natural electron configurations "[core] 5d (9.98) 6p (0.02)" and "[core] 6s (1.78) 5d (9.99) 6p (0.23)", respectively. By removing the external electric field, the cationic and anionic gold atoms reconfigure their charge distribution and relax to "[core] 5d (10.00)" and "[core] 6s (2.00) 5d (10.00)", respectively.

Figure 3a shows the effect of external electric field on the highest occupied-lowest unoccupied molecular orbitals of gold dimer. According to this Figure, at the low magnitudes of external field (0 to 0.0050 au), the energies of HOMO and LUMO remain unchanged. Then, gradual lowering of energy for the both HOMO and LUMO is observed for the field of larger magnitudes (0.0050 to 0.0395 au). However, for higher magnitudes of electric field, LUMO is relatively more susceptible to variation in energy levels than HOMO. A similar behavior is observed for the Lithium dimer, i.e., LUMO is also more sensitive to the variation in electron density than HOMO [57]. The plot of band gap energy ($E_g = E_{LUMO} - E_{HOMO}$) versus the external electric field is depicted in Figure 3b. This curve shows that the minimum band gap energy of gold dimer, i.e., E_g = 6.624 eV, can be achieved for electric field value of 0.0395 au.

Table 3. *Natural electron configuration of gold dimer in the absence and presence of external electric field.*

Field (au)	Atom number	② ⟹ ①
0.0000	1	[core] 6S(1.01) 5d(9.96) 6p(0.03)
	2	[core] 6S(1.01) 5d(9.96) 6p(0.03)
0.0050	1	[core] 6S(1.15) 5d(9.96) 6p(0.03)
	2	[core] 6S(0.88) 5d(9.96) 6p(0.03)
0.0100	1	[core] 6S(1.29) 5d(9.96) 6p(0.02)
	2	[core] 6S(0.74) 5d(9.96) 6p(0.03)
0.0150	1	[core] 6S(1.42) 5d(9.96) 6p(0.02)
	2	[core] 6S(0.61) 5d(9.96) 6p(0.03)
0.0200	1	[core] 6S(1.54) 5d(9.96) 6p(0.01) 7p(0.01)
	2	[core] 6S(0.49) 5d(9.96) 6p(0.03)
0.0250	1	[core] 6S(1.65) 5d(9.96) 6p(0.01) 7p(0.01)
	2	[core] 6S(0.37) 5d(9.96) 6p(0.03)
0.0300	1	[core] 6S(1.74) 5d(9.97) 6p(0.01) 7p(0.02)
	2	[core] 6S(0.27) 5d(9.97) 6p(0.02)
0.0350	1	[core] 6S(1.81) 5d(9.97) 6p(0.05) 7p(0.01)
	2	[core] 6S(0.17) 5d(9.97) 6p(0.02)
0.0390	1	[core] 6S(1.84) 5d(9.98) 6p(0.09) 7p(0.01)
	2	[core] 6S(0.08) 5d(9.98) 6p(0.02)
0.0395	1	[core] 6S(1.85) 5d(9.98) 6p(0.10) 7p(0.01)
	2	[core] 6S(0.07) 5d(9.98) 6p(0.02)

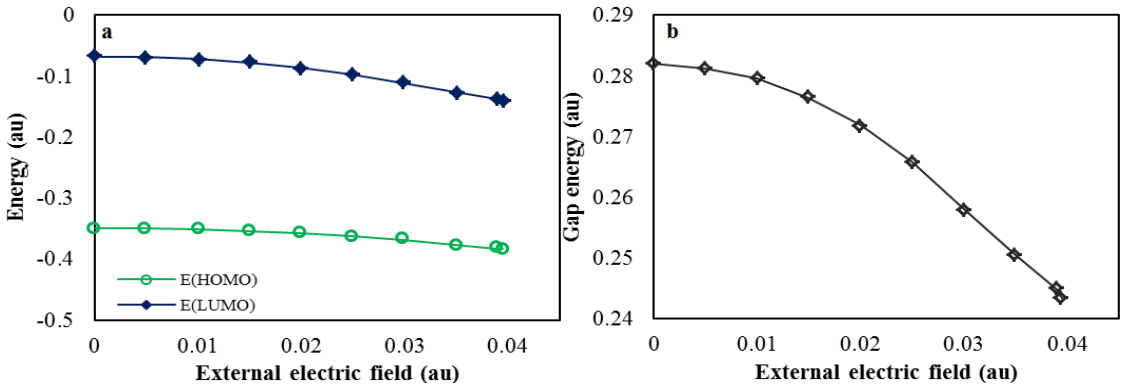

Figure 3. *Effect of external electric field on the a) HOMO and LUMO energy levels, and b) gap energy of Au_2 molecule.*

3.1.2. The Effect of External Electric Field on the Gap Energies of Au_{3-10}

The gold clusters Au_8 and Au_9 are transition state structures in the presence of weak electric fields perpendicular to the molecular plane; hence, the geometries of Au_{3-10} are optimized in the presence of relatively weak external electric fields along the directions perpendicular ($F_{\perp}$) and parallel to the molecular plane ($F_{\rightarrow}$ and $F_{\downarrow}$) and the frontier orbital (HOMO-LUMO) gap energies of these clusters in the absence (F=0) and presence of electric fields ($F_{\perp} = F_{\rightarrow} = F_{\downarrow}$ =0.0050 and 0.0100 au; 0.001 au = 0.05142 V/A° [55]) are summarized in Table 4. The HOMO-LUMO gap energy of a molecule is considered to be important electronic property which can represent its ability to participate in a chemical reaction. As Table 4 represents, the application of external electric field can increase or decrease the gap energy of neutral gold clusters depending on the direction and magnitude of the applied field. When the external electric field decreases the HOMO-LUMO gap energy of a cluster along a particular direction, a more reactive gold cluster can be obtained. However, according to Table 4, the HOMO-LUMO gap energy of the clusters Au_3, Au_4, Au_6, Au_9 and Au_{10} has increased along some directions of the applied electric field. In the case of Au_{10}, the gap energy shows gradual increase along the direction perpendicular to the molecular plane ($F_{\perp}$ =0.0050 au, E_g = 5.678 eV) and then decreases ($F_{\perp}$ =0.0100 au, E_g = 5.665 eV) that is only 0.0110 eV lower in energy than its zero field gap energy value of 5.676 eV.

In order to know the behavior of the increasing HOMO-LUMO gap energy of Au_3, Au_4, Au_6 and Au_9, we compute the gap energies of these clusters as a function of electric field. For Au_4 and Au_9 clusters, the increase in external electric field along the direction parallel to the molecular plane ($F_{\rightarrow}$) results in threshold gap energy values of 5.801 eV ($F_{\rightarrow}$ = 0.0250 au) and 4.252 eV ($F_{\rightarrow}$ = 0.0150 au) that are not very different from their zero field gap energy values of 5.843 eV and 4.306 eV, respectively. However, the calculations reveal that in spite of gradual increase in the HOMO-LUMO gap energy in the presence of lower electric fields, the gold trimer and hexamer can result in more reactive clusters as the external electric field increases. Figure 4a depicts the gap energy of gold trimer versus the applied electric field along the direction parallel to the molecular plane ($F_{\rightarrow}$). As this Figure shows, the external electric field increases the gap energy of Au_3 up to 5.092 eV ($F_{\rightarrow}$ = 0.0150 au) and then suddenly decreases to its minimum threshold band gap energy value of 3.574 eV ($F_{\rightarrow}$ = 0.0300 au), that is 1.300 eV lower in energy than its zero field gap energy. The gold trimer dissociates at the electric field value of 0.0350 au. A similar behavior is observed for the gold hexamer in Figure 4b. According to this Figure, as the external electric field increases along the direction perpendicular to the molecular plane, the band gap energy of gold hexamer shows gradual increase from 7.510 eV (F = 0) to 7.571 eV ($F_{\perp}$ = 0.0250 au) and then abruptly decreases to its minimum threshold band gap energy value of 4.850 eV ($F_{\perp}$ = 0.0400 au), that is 2.660 eV lower in energy than its zero electric field value. The gold hexamer dissociates at the external electric field value of 0.0450 au.

Table 4. *The frontier orbital (HOMO-LUMO) gap energies (Eg/eV) of neutral gold clusters Au_{3-10} in the absence (F=0) and presence of electric fields ($F_{\perp} = F_{\rightarrow} = F_{\downarrow}$ =0.0050 and 0.0100 au). The parentheses indicate the difference of gap energies in the absence and presence of electric field.*

	F=0	**$F_{\rightarrow}$=0.005**	**$F_{\rightarrow}$=0.010**	**$F_{\downarrow}$=0.005**	**$F_{\downarrow}$=0.010**	**$F_{\perp}$=0.005**	**$F_{\perp}$=0.010**
Au_3	4.874	4.932 (0.058)	5.049 (0.175)	4.788 (-0.086)	4.676 (-0.198)	4.872 (-0.002)	4.865 (-0.009)
Au_4	5.843	5.849 (0.006)	5.859 (0.016)	5.832 (-0.011)	5.796 (-0.047)	5.840 (-0.003)	5.833 (-0.010)
Au_5	4.801	4.794 (-0.007)	4.773 (-0.028)	4.780 (-0.021)	4.741 (-0.060)	4.798 (-0.003)	4.795 (-0.006)
Au_6	7.510	7.390 (-0.120)	7.168 (-0.342)	7.399 (-0.111)	7.226 (-0.284)	7.513 (0.003)	7.519 (0.009)
Au_7	4.650	4.643 (-0.007)	4.612 (-0.038)	4.639 (-0.011)	4.591 (-0.059)	4.647 (-0.003)	4.644 (-0.006)
Au_8	6.135	6.058 (-0.077)	5.831 (-0.304)	6.057 (-0.078)	5.763 (-0.372)	TS	TS
Au_9	4.306	4.343 (0.037)	4.342 (0.036)	4.298 (-0.008)	4.271 (-0.035)	4.306 (0.000)	TS
Au_{10}	5.676	5.633 (-0.043)	5.526 (-0.150)	5.648 (-0.028)	5.557 (-0.119)	5.678 (0.002)	5.665 (-0.011)

"TS" indicates transition state structures.

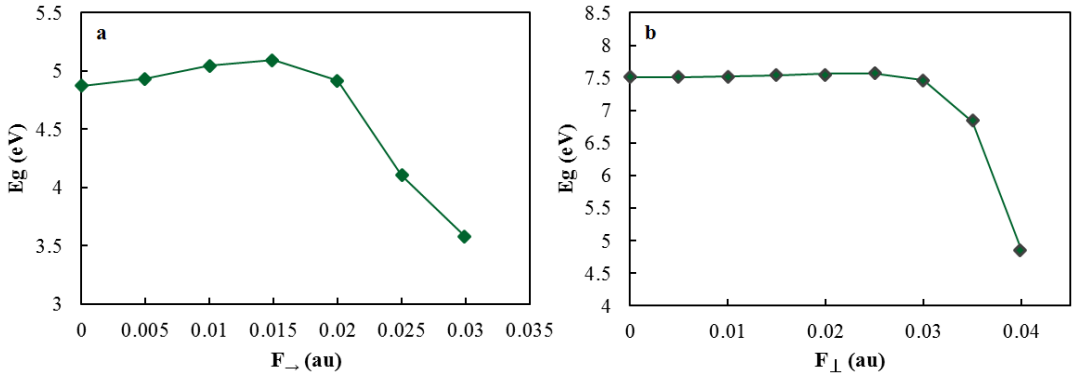

Figure 4. *The frontier orbital (HOMO-LUMO) gap energy of a) Au_3 along the direction of electric field parallel to the molecular plane and b) Au_6 along the direction of electric field perpendicular to the molecular plane.*

The results represented in Figure 4 state an important consequence, i.e., by correctly controlling the direction and magnitude of the applied external electric field, highly reactive gold clusters with low energy gaps can be achieved. To better understand the effect of external electric field on the charge distribution of the gold trimer and hexamer, we perform natural population analysis in the presence of their threshold electric fields, i.e., $F_{\rightarrow}$ =0.0300 au and $F_{\perp}$ = 0.0400 au, respectively; and compare the obtained results with their zero field charges. Figure 5 represents the natural charges and total electron density contour maps of gold trimer and hexamer in the absence and presence of the applied field along the directions parallel and perpendicular to the molecular plane, respectively.

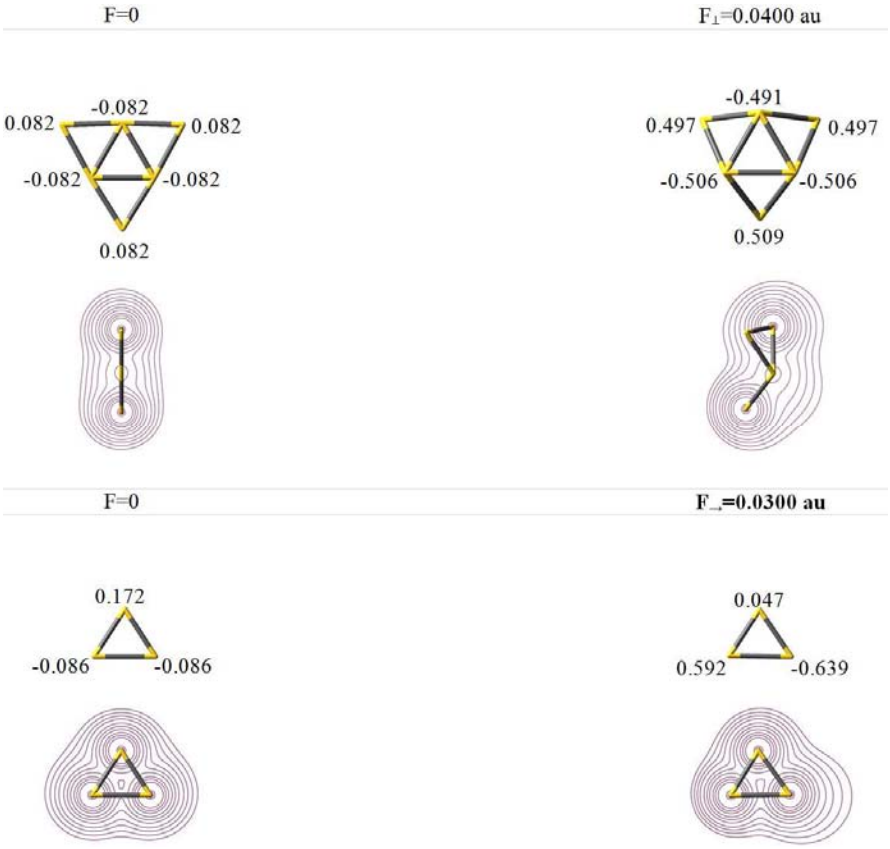

Figure 5. *Natural charges and total electron density contour maps of Au_6 and Au_3 in the absence and presence of external electric field along the directions perpendicular and parallel to the molecular plane, respectively.*

It is clear that the external electric field changes the geometry of the clusters and pushes their electronic cloud along the direction of the applied field. In the presence of electric field along the direction perpendicular to the molecular plane, the planar gold hexamer transforms to a three-dimensional structure. A non-planar cluster has more spatial opportunities to interact with other nucleophilic and electrophilic species. Furthermore, in the presence of external electric field, more charge separations and stronger nucleophilic and electrophilic sites are achieved. As a result, the reactivity of a cluster in the presence of external electric field can increase not only due to decrease in its gap energy, but also because of the change in its geometry, electron distribution and charge separations.

As we will see in the next sections, the application of an external electric field along the directions parallel to the molecular plane may have considerable effect on the second-order hyperpolarizability of gold hexamer. Au_6 is a totally symmetric D_{3h} triangle in the absence of the applied field; however, in the presence of external electric field along the directions parallel to the molecular plane, reduces its symmetry from a totally symmetric D_{3h} equilibrium geometry to a lower symmetry C_{2v} structure. Figures 6 and 7 present the frontier molecular orbitals of gold hexamer together with the corresponding contour maps in the absence ($F = 0$) and presence of electric field parallel to the molecular plane ($F_{\rightarrow} = F_{\downarrow} = 0.0100$ au).

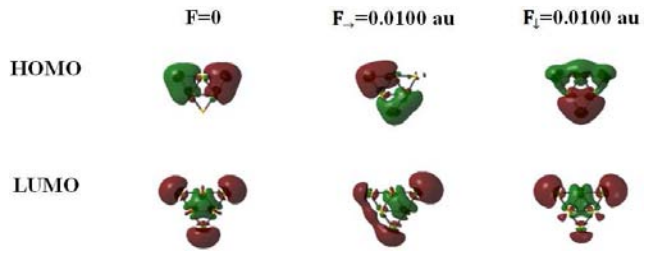

Figure 6. *The frontier molecular orbitals (HOMO and LUMO) of neutral gold hexamer in the absence (F=0) and presence of electric field parallel to the molecular plane ($F_{\rightarrow} = F_{\downarrow} = 0.0100$ au).*

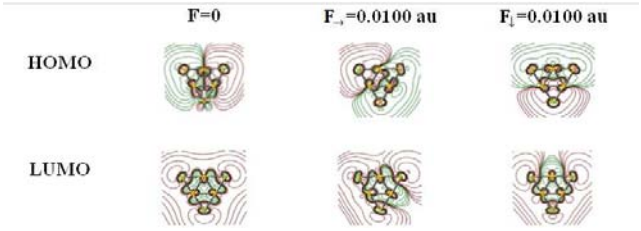

Figure 7. *The frontier molecular orbital (HOMO and LUMO) contour maps of neutral gold hexamer in the absence (F=0) and presence of electric field parallel to the molecular plane ($F_{\rightarrow} = F_{\downarrow}$ = 0.0100 au).*

As these Figures illustrate, the application of external electric field parallel to the molecular plane breaks the symmetry of frontier orbitals due to polarization of the gold hexamer in the presence of the applied field and pushes the lobes of the highest occupied-lowest unoccupied molecular orbitals (HOMO-LUMO) along the direction of the field.

3.2. Nonlinear Optical Properties

3.2.1. Frequency-Dependent First-order Hyperpolarizability for Neutral Gold Clusters

Materials with non-linear optical (NLO) activity are those in which a non-linear polarization of light occurs during the application of an intense electric field, which is caused by the exposure of the material to a laser beam [48]. The first important controlling factor for the static first-order hyperpolarizability is the symmetry of the cluster, i.e., the first-order hyperpolarizability tensor vanishes for the centrosymmetric molecules [48]. The geometry, size and dimensionality of a cluster may be another important determining factor due to the extensivity and flexibility of the electronic cloud. Wang et al. [58] calculated dipole moments and polarizabilities of Ge_n (n=2-25) clusters under B3LYP/LANL2DZ scheme and concluded that the polarizability of the cluster is not only dependent on HOMO-LUMO gap but also closely related to geometrical characteristics. For instance, the HOMO-LUMO gap of Ge_{18} is larger than that of Ge_{19}, while the polarizability of the former is larger than that of the latter due to the structural difference. Furthermore, in the base of sum-over-states (SOS) approach, the following expression can be used for the static case [59, 60],

$$\beta \propto \frac{\Delta\mu_{gm} f_{gm}}{E_{gm}^3} \quad (7)$$

where $\Delta\mu_{gm}$ is the change in dipole moment between the ground and mth excited state, f_{gm} is the oscillator strength of the transition from ground state to the mth excited state and E_{gm} is transition energy. According to this relation, for any non-centrosymmetric system, small value of transition energy with large oscillator strength would be favorable. Table 5 contains the calculated static first-order hyperpolarizability $\beta(0;0,0)$ and second harmonic generation $\beta(-2\omega;\omega,\omega)$ coefficients for the neutral gold clusters and Figure 8a presents the variation in the static first-order hyperpolarizability $\beta(0;0,0)$ versus the cluster size.

Table 5. *Static first-order hyperpolarizability β(0;0,0) and second harmonic generation $\beta(-2\omega;\omega,\omega)$ coefficients for the neutral gold clusters (λ=800 nm, β in 10^{-30} esu).*

n	β(0;0,0)	β(-2ω;ω,ω)
2	0.00000	0.00000
3	7.26128	2.60940
4	0.00002	0.00049
5	4.81059	5.91001
6	44.4980	17.3952
7	138.002	184.283
8	0.00222	0.00348
9	20.6197	60.2401
10	0.00000	0.00000

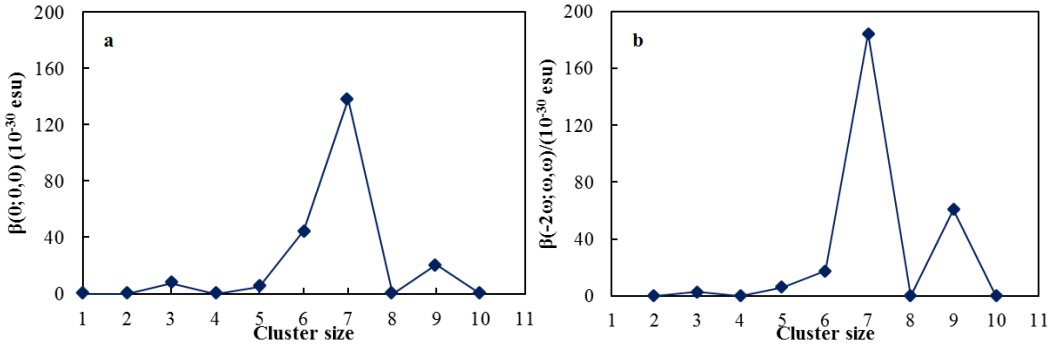

Figure 8. *a) Static first-order hyperpolarizability β(0;0,0), and b) second-harmonic generation $\beta(-2\omega;\omega,\omega)$ at optical wavelength 800 nm, versus the cluster size.*

Here, we perform a time-dependent density functional calculation (TD-DFT) and present the maximum and lowest-energy excitation wavelengths along with their corresponding energies, oscillator strengths, dominant molecular orbital transitions and ground to excited state transition electric dipole moments of gold clusters Au_{2-10} in Table 6. As this Table illustrates, the highest occupied-lowest unoccupied molecular orbital (HOMO-LUMO) transitions have no effect on the excitations of Au_4, Au_8, and Au_{10} clusters. Moreover, according to Figure 8a, due to centrosymmetric geometries of Au_2, Au_4 and Au_{10} clusters, the static first-order hyperpolarizability coefficient for these structures is zero. Furthermore, $\beta(0;0,0)$ value for Au_8 with C_s symmetry is too low (0.00222×10^{-30} esu), while its value for centrosymmetric

gold octamer with D_{2h} symmetry is zero. As Table 6 shows, HOMO-LUMO transitions have more important effect on the lowest-energy excitations of Au_2, Au_3, Au_5, Au_6, Au_7 and Au_9 clusters and the non-centrosymmetric Au_3, Au_5, Au_6, Au_7 and Au_9 clusters have nonzero static first-order hyperpolarizability coefficients (Table 5). As can be seen in Table 6, the small triangular gold trimer has the lowest excitation energy value of 0.3938 eV; however, its static first-order hyperpolarizability is only 7.26128×10^{-30} esu, that may be due to its small oscillator strength value of 0.0036.

Table 6. *Maximum absorption wavelength (λ_{max}/nm), lowest-energy absorption wavelength (λ_{LE}/nm) together with their corresponding excitation energies (E_{exc}/eV), oscillator strengths (f), dominant molecular orbital transitions and ground to excited state transition electric dipole moments (TDM/au.).*

n	λ_{LE}	E_{exc}	f	MO transition	TDM	λ_{max}	E_{exc}	f	MO transition	TDM
2	398.44	3.1117	0.2436	H→L (90%)	1.7877	181.47 nm	6.8322 eV	1.0763	H→L (10%) H-1→L+3 (11%) H-2→L+1 (30%) H-3→L+2 (30%)	2.5358
3	3148.7	0.3938	0.0036	H→L (100%)[a]	0.6132	295.27 nm	4.1990 eV	0.1763	H-10→L (19%) H→L (7%)[b] H→L+3 (73%)[a]	1.3092
4	374.03	3.3149	0.5932	H→L+1 (88%)	2.7027	203.59 nm	6.0898 eV	1.0387	H-4→L+2 (62%) H-14→L (19%)	2.6385
5	850.05	1.4586	0.0034	H→L (92%)[b]	0.3069	341.73 nm	3.6281 eV	0.3520	H-1→L (27%)[a] H→L+1 (21%)[b] H-13→L (13%)[b]	1.9901
6	345.74	3.5861	0.3912	H→L (70%)	2.1100	345.74 nm	3.5861 eV	0.3912	H→L (70%)	2.1100
7	694.23	1.7859	0.0035	H→L (73%)[a] H→L (15%)[b]	0.2844	418.64 nm	2.9616 eV	0.2417	H→L+2 (46%)[a] H→L+1 (18%)[b]	1.8252
8	370.14	3.3496	0.0074	H-4→L (37%) H-2→L (54%)	0.3010	349.08 nm	3.5518 eV	0.4223	H-1→L (82%)	2.2030
9	1107.4 862.49	1.1196 1.4375	0.0073 0.0180	H→L (100%)[b] H→L (100%)[a]	0.5147 0.7154	380.37 nm	3.2595 eV	0.3283	H-1→L+1 (16%)[a] H-11→L (30%)[b]	2.0277
10	534.90	2.3179	0.0220	H-1→L+1 (49%) H→L+2 (51%)	0.6224	400.57 nm	3.0952 eV	0.6539	H-1→L+1 (40%) H→L+2 (41%)	2.9366

For the open shell structures, "a" and "b" indicate "α spin→α spin" and "β spin→β spin" molecular orbital transitions, respectively.

The highly asymmetric gold heptamer Au_7 has the highest static first-order hyperpolarizability value of 138.002×10^{-30} esu. According to Table 6, the lowest excitation energy of Au_7 is relatively small (1.7859 eV) that can enhance its first-order hyperpolarizability coefficient, however, it appears that the asymmetric geometry and extensivity of its electronic cloud would play considerable role in its high first-order hyperpolarizability coefficient. In the case of Au_9, the two lowest excitations with energies 1.1196 and 1.4375 eV are responsible for the "β spin→β spin" and "α spin→α spin" HOMO-LUMO transitions, respectively. The low excitation energy values of 1.1196 and 1.4375 eV, together with the distributed electronic cloud may result in the first-order hyperpolarizability value of 20.6197×10^{-30} esu. For the gold hexamer, the maximum absorption is also the lowest-energy excitation and in spite of its highest HOMO-LUMO gap energy, this non-centrosymmetric cluster shows relatively high static first-order hyperpolarizability value of 44.498×10^{-30} esu. According to Table 6, the HOMO-LUMO transition contribution to the lowest-energy excitation of Au_6 is about 70% and regarding its relatively high excitation energy value of 3.5861 eV, it has also high oscillator strength and transition electric dipole moment values of 0.3912 and 2.1100 au., respectively; that can enhance its static first-order hyperpolarizability.

The second-harmonic generation (SHG) is a special case of sum-frequency generation. In the second-harmonic generation (SHG), two photons at frequency ω combine to form a photon at frequency 2ω. In other words, second harmonic generation conserves energy [48]. Figure 8b displays the variation in the second-harmonic generation (SHG) coefficient of gold clusters with increasing cluster size at the wavelength of 800 nm. By comparing Figures 8a and 8b, we find similar trend for the variation of static first-order hyperpolarizability and second-harmonic generation with the increasing cluster size. Furthermore, the calculated second-harmonic generation of Au_9 (60.2401×10^{-30} esu) is comparable with that of protected $Au_{10}(SG)_{10}$ cluster (85×10^{-30} esu) [22]; however, the calculated $\beta(-2\omega;\omega,\omega)$ value of gold heptamer Au_7 (184.283×10^{-30} esu) is even higher than second-harmonic generation of protected $Au_{10}(SG)_{10}$ at the wavelength of 800 nm [22], indicating the fact that the smaller clusters should exhibit higher hyperpolarizabilities than larger particles [17].

The second harmonic generation coefficient $\beta(-2\omega;\omega,\omega)$ for $Au_{2\text{-}10}$ with ω varying from 0.00 to 1.63 eV are represented in Table 7. As can be seen in this Table, moving from ω=0 to 1.63 eV, the variation in second-harmonic generation (SHG) is more important for Au_5, Au_7 and Au_9 clusters; hence, the frequency dispersion in the coefficients of these nanoclusters are depicted in Figure 9a. The maximum absorptions of Au_5 and Au_9 are around 3.6281 and 3.2595 eV, respectively; and the sharp increase in SHG around 1.2-1.6 eV is an indication of two-photon resonance and so our calculated values of second-harmonic generation are in good agreement. The dispersion plot in

Figure 9a for Au_7 exhibits a maximum around 1.36 eV and a modest normal increase in SHG values up to this point compared to Au_5 and Au_9 in the same energy region meaning no resonance effect for Au_7.

Table 7. *Dynamic second harmonic generation coefficients for Au_{2-10} (β in 10^{-30} esu).*

n	λ (nm)					
	759.4	**911.3**	**1139.1**	**1518.8**	**2278.2**	**4556.3**
	β(-2ω ;ω ,ω)					
2	0.00000	0.00000	0.00000	0.00000	0.00000	0.00000
3	4.81593	3.21151	2.43926	3.99948	13.4516	52.7974
4	0.00256	0.00016	0.00008	0.00006	0.00005	0.00004_5
5	1108.32	18.1939	2.29157	5.34843	5.05266	4.35720
6	23.1174	11.8241	8.51323	6.90519	6.03528	5.59202
7	31.6396	217.452	14.8066	13.9783	5.97521	4.88071
8	0.00024	0.02240	0.00100	0.00085	0.00075	0.00069
9	805.567	377.682	100.173	6.33580	43.7746	22.9408
10	0.00000	0.00000	0.00000	0.00000	0.00000	0.00000

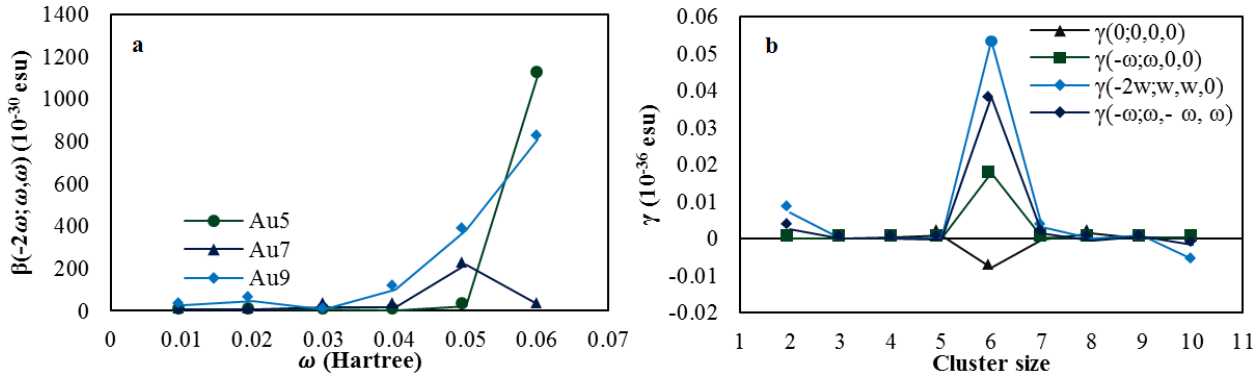

Figure 9. *a) Dispersion curves of second-harmonic generation coefficients for Au_5, Au_7 and Au_9 and b) static second-order hyperpolarizability $\gamma(0;0,0,0)$, Optical-Kerr $\gamma(-\omega;\omega,0,0)$, electric-field induced second-harmonic generation $\gamma(-2\omega;\omega,\omega,0)$ and degenerate four-wave mixing $\gamma(-\omega;\omega,-\omega,\omega)$ coefficients as a function of cluster size.*

3.2.2. Frequency-Dependent Second-Order Hyperpolarizability for Neutral Gold Clusters

Table 8 lists the calculated static second-order hyperpolarizability $\gamma(0;0,0,0)$, Optical-Kerr $\gamma(-\omega;\omega,0,0)$, electric-field induced second-harmonic generation $\gamma(-2\omega;\omega,\omega,0)$ and degenerate four-wave mixing $\gamma(-\omega;\omega,-\omega,\omega)$ coefficients of neutral gold clusters. The calculated values of the second-order hyperpolarizability coefficients $\gamma(0;0,0,0,)$, $\gamma(-\omega,\omega,0,0)$, $\gamma(-2\omega;\omega,\omega,0)$ and $\gamma(-\omega;\omega,-\omega,\omega)$ as a function of cluster size are represented in Figure 9b. It is clear that the gold hexamer exhibits the highest second-order hyperpolarizability coefficients at the wavelength of 800 nm. Furthermore, the second-order hyperpolarizability for Au_6 displays the trend of increasing magnitude from static $\gamma(0;0,0,0)$ to Kerr effect $\gamma(-\omega;\omega,0,0)$ to degenerate four-wave mixing $\gamma(-\omega;\omega,-\omega,\omega)$ to electric field induced second-harmonic generation $\gamma(-2\omega;\omega,\omega,0)$. For the gold hexamer, the maximum absorption is also the lowest-energy excitation and this cluster with the largest HOMO-LUMO gap energy has a highly symmetric D_{3h} structure in the absence of external electric field; however, the applied field breaks its symmetry and as Figures 5, 6 and 7 show, results in more flexible electronic cloud. To better know the reason for the observed high second-order hyperpolarizability of gold hexamer, the energy levels of neutral gold clusters Au_{2-10} in the absence and presence of external electric field along the directions parallel and perpendicular to the molecular plane are also depicted in Figure 10.

Table 8. *The static second-order hyperpolarizability $\gamma(0;0,0,0)$, Optical-Kerr $\gamma(-\omega;\omega,0,0)$, electric-field induced second-harmonic generation $\gamma(-2\omega;\omega,\omega,0)$ and degenerate four-wave mixing $\gamma(-\omega;\omega,-\omega,\omega)$ of Au_{2-10} (λ=800 nm, γ in 10^{-36} esu).*

n	γ(0;0,0,0)	γ(-ω;ω,0,0)	γ(-2w;w,w,0)	γ(-ω;ω,- ω, ω)
2	-0.36357	10.7901	7082.61	2371.78
3	-73.6792	17.8723	57.4777	61.5913
4	135.702	18.3988	66.1347	-4.79030
5	808.878	-8.03727	2.04751	-276.981
6	-8019.95	17708.6	53368.3	38171.4
7	-277.000	321.296	3114.79	1451.89
8	1428.31	-118.404	-187.219	-656.914
9	56.5822	139.390	715.761	359.116
10	39.7869	181.809	-5738.53	-1744.30

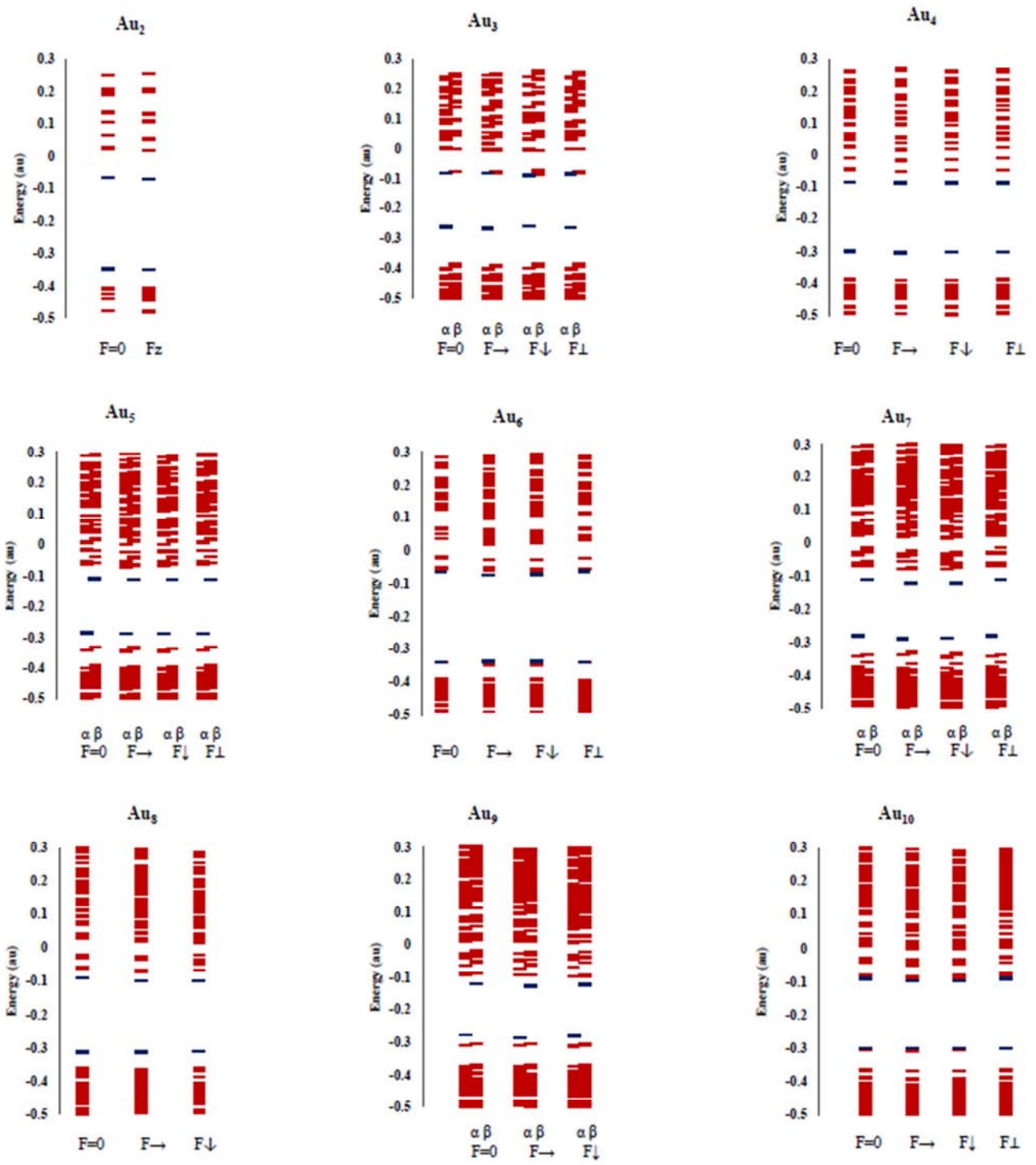

Figure 10. *Energy levels of neutral gold clusters $Au_{2\text{-}10}$ in the absence and presence of external electric field along the directions parallel and perpendicular to the molecular plane ($F_{\rightarrow}=F_{\downarrow}=F_{\perp}=0.0100$ au).*

As this Figure exhibits, the external electric field has negligible effect on the energy levels of Au_2, Au_3, Au_4, Au_5 and Au_9; whereas, its influence on the energy levels of Au_8 is relatively small, resulting in $\gamma(0;0,0,0)$ value of 1428.31×10^{-36} esu. In the case of Au_7, the decrease in the energies of HOMO and LUMO is nearly the same, so its gap energy remains nearly unaltered. However, it is obvious that the applied field has considerable effect on the virtual orbitals of gold hexamer and decreases the energy of these orbitals in the directions parallel to the molecular plane ($F_{\rightarrow}$ and $F_{\downarrow}$). To better understand, the density of states (DOS) plots for Au_4, Au_5 and Au_6 in the absence and presence of external electric field along the direction parallel to the molecular plane are compared in Figure 11. By comparison, a red-shift for the virtual orbitals of Au_6 can be observed, i.e., the applied field has more important effect on the virtual orbitals of gold hexamer and decreases the energies of these orbitals more, resulting in smaller HOMO-LUMO gap energy in the

presence of external electric field parallel to the molecular plane. In order to know the consequences of the decrease in the energy of virtual orbitals of gold hexamer due to the applied field, a time-dependent density functional (TD-DFT) calculation is also performed on Au_6, in the absence and presence of external electric field and the corresponding UV-Vis spectra are presented in Figure 12. As can be seen in this Figure, the applied field along the directions parallel to the molecular plane results in a red-shift for the allowed excitations and appearing additional spectroscopic line in the low-energy region of the UV-Vis spectra of gold hexamer.

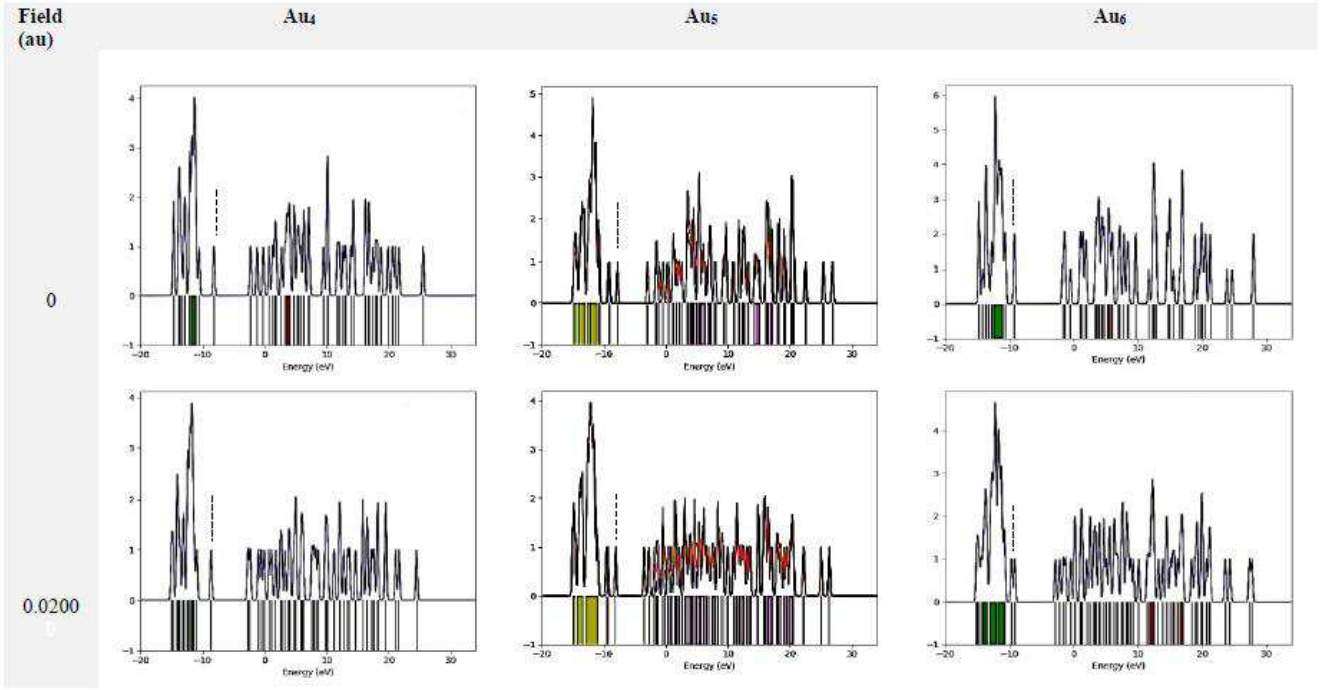

Figure 11. *Density of states (DOS) plots for Au_4, Au_5 and Au_6 in the absence and presence of external electric field along the direction parallel to the molecular plane ($F_{\rightarrow}$=0.0200 au). The full width at half-maximum of the Gaussian curves are 0.3 eV. The dashed line represents the highest-occupied molecular orbital (HOMO).*

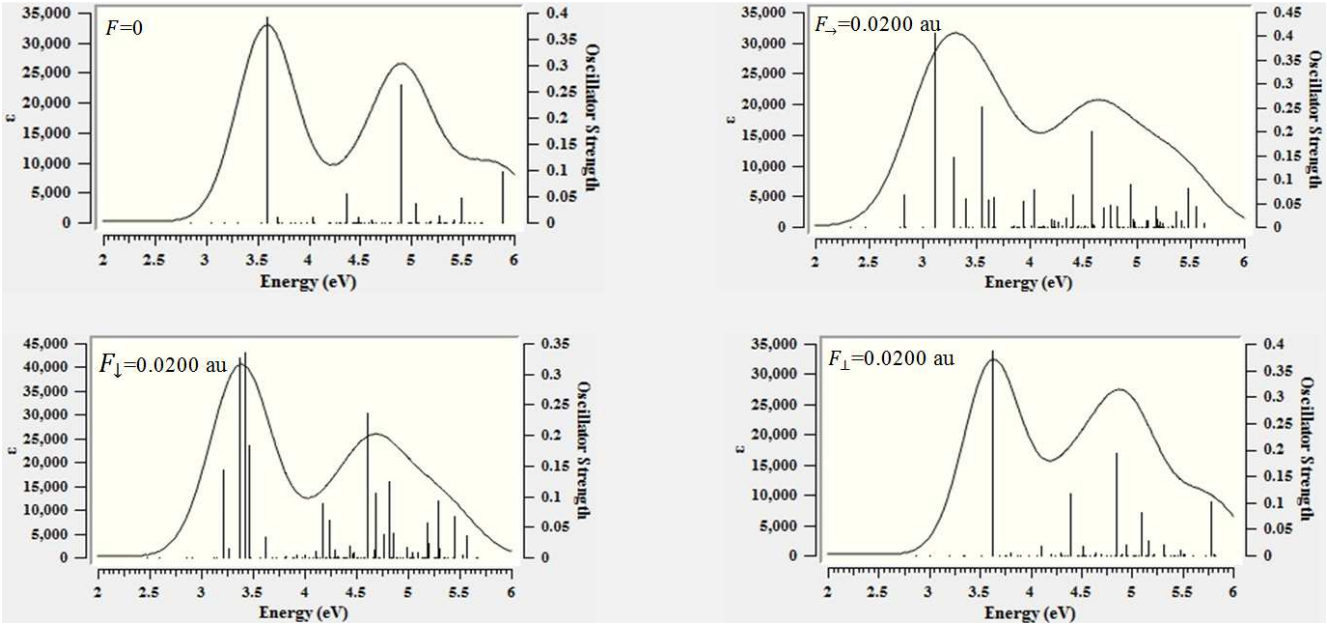

Figure 12. *UV-Vis spectra of neutral gold hexamer in the absence and presence of external electric field.*

The effect of external electric field on the UV-Vis spectrum of gold hexamer is also presented in Figure 13. As this Figure shows, by increasing the external electric field, the energy of allowed excitations decreases, resulting in more flexible electronic cloud and better response to the applied field. The allowed molecular orbital transitions of the additional

spectroscopic line together with the corresponding excitation energies, wavelengths and oscillator strengths are presented in Figure 14. It appears that these low-energy excitations of gold hexamer in the presence of external electric field play important role in the high second-order hyperpolarizability of this cluster. In summary, in the case of gold hexamer, the maximum absorption is also the lowest-energy excitation and regarding its high HOMO-LUMO gap energy in the absence of external electric field, the applied field has considerable effect on the non-linear response of this cluster due to changing its geometry, breaking its D_{3h} symmetry, a red-shift for the allowed excitations and appearing additional low-energy excitations that would result in more flexible electronic distribution and better response to the applied field.

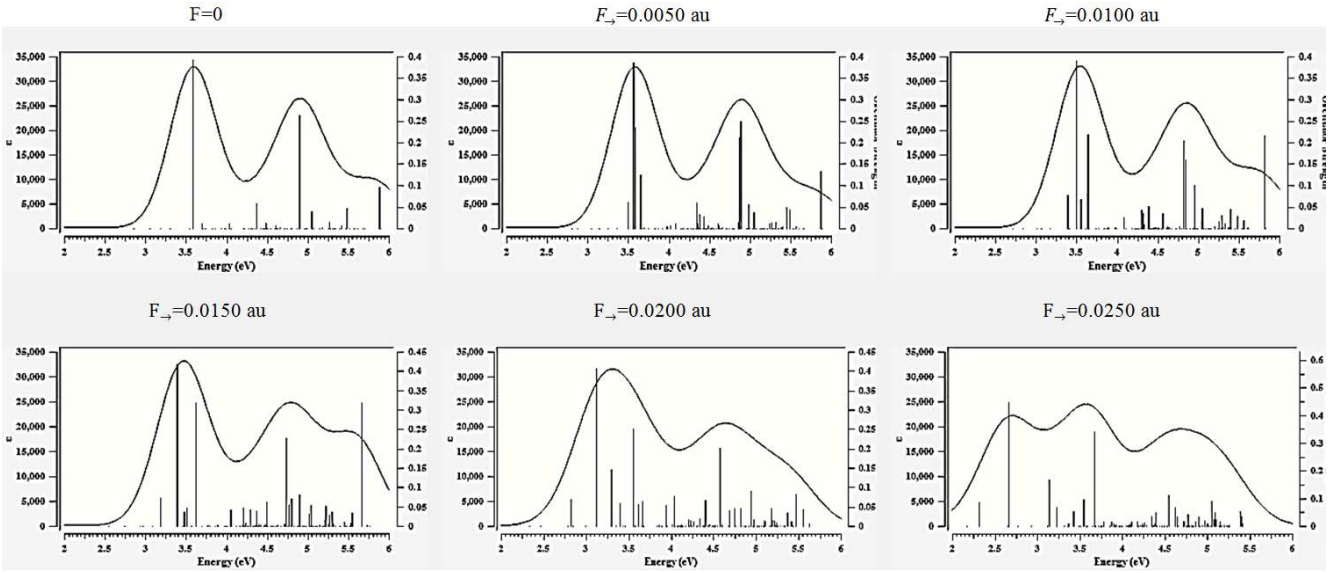

Figure 13. *The effect of external electric field on the UV-Vis spectrum of gold hexamer.*

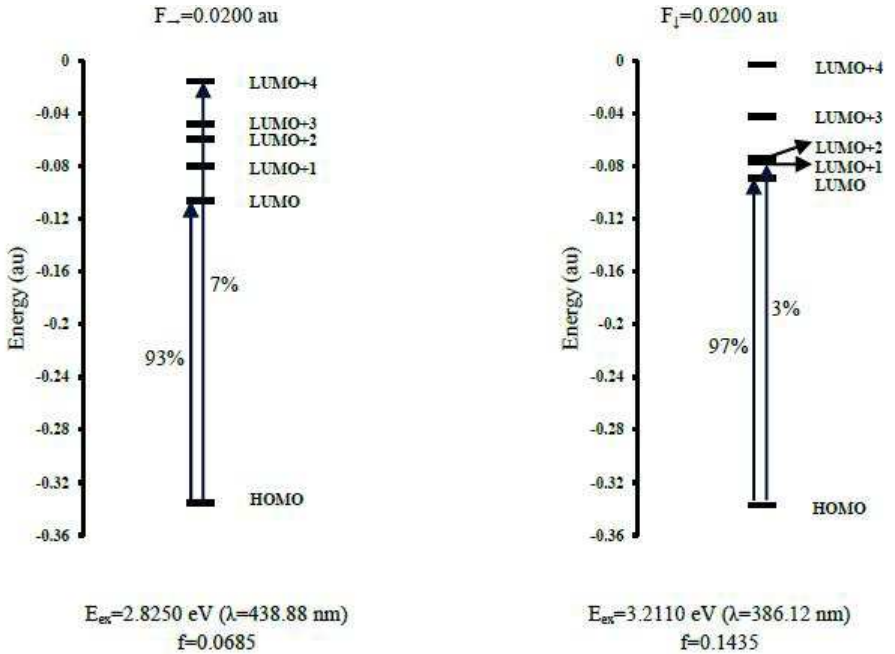

Figure 14. *Molecular orbital transitions of the additional spectroscopic line of Au_6 in the presence of external electric field along the directions parallel to the molecular plane together with the corresponding excitation energies, wavelengths and oscillator strengths.*

The incident-frequency effect on the second-order hyperpolarizability of neutral gold clusters is also examined. The electro-optical-Kerr effect (EOKE) $\gamma(-\omega;\omega,0,0)$ and electric-field-induced second-harmonic generation (EFISHG) $\gamma(-2\omega;\omega,\omega,0)$ coefficients for $Au_{2\text{-}10}$ with ω varying from 0.00 to 1.63 eV are represented in Table 9 and the frequency dispersion of these coefficients are depicted in Figure 15. The dispersion plot in this Figure is more important for gold hexamer, so that the electro-optical Kerr effect (EOKE) $\gamma(-\omega;\omega,0,0)$ and electric-field-induced second-harmonic generation (EFISHG) $\gamma(-2\omega;\omega,\omega,0)$ coefficients of Au_6 disperse and increase to a different extent. In particular,

moving from ω =0.00 to 1.63 eV, the value of second-order hyperpolarizability increases by 2.31 times for EOKE and 9.32 times for EFISHG. In fact, the electro-optical Kerr effect (electric-field-induced second-harmonic generation) begins to disperse and exhibits a large value owing to the one-photon (two-photon) resonance that occurs when ω (2ω) is close to the strong allowed transition energy. For the Au_6 cluster, the calculated first-strong allowed transition energy is about 3.5861 eV. As a result, at ω =1.793 eV the near two-photon resonance results in a higher dispersion in the electric-field-induced second-harmonic generation value. In the case of $Si_{10}H_{16}$ cluster, the calculated first-strong allowed transition energy is around 6.53 eV, i.e., at ω =3.2 eV the near two-photon resonance would result in a large dispersion in the $\gamma(-2\omega;\omega,\omega,0)$ values [61]. In summary, these results show that the third-order non-linear (NLO) properties of gold hexamer are strongly affected by the frequency of incident light, and thus can be tuned using the incident frequency for applications.

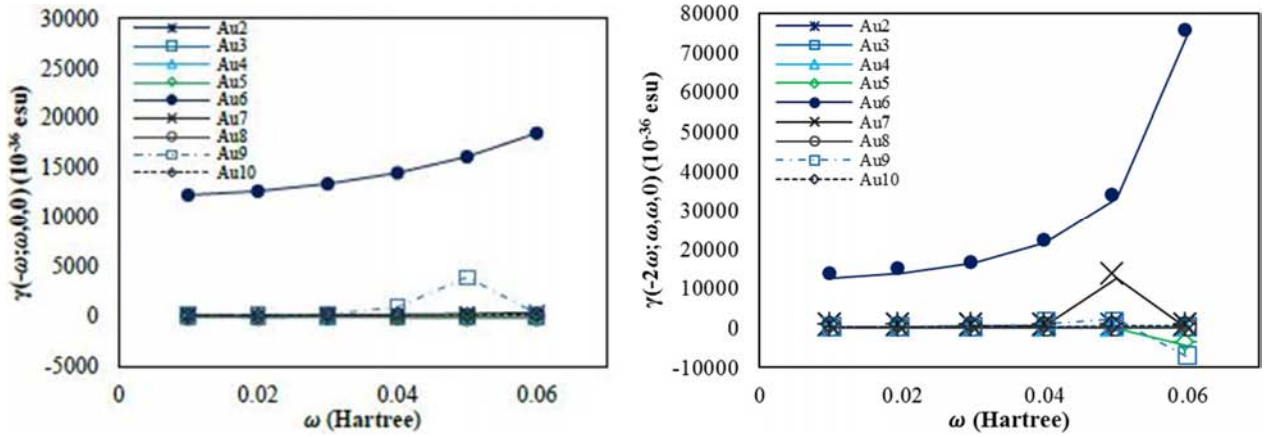

Figure 15. *Dispersion curves of electro-optical-Kerr effect (EOKE) $\gamma(-\omega;\omega,0,0)$ and electric-field-induced second-harmonic generation (EFISHG) $\gamma(-2\omega;\omega,\omega,0)$ coefficients for neutral gold clusters Au_{2-10}.*

Table 9. *Dynamic second-order hyperpolarizability coefficients for Au_{2-10} (γ in 10^{-36} esu).*

n	λ (nm)					
	759.4	**911.3**	**1139.1**	**1518.8**	**2278.2**	**4556.3**
	$\gamma(-\omega;\omega,0,0)$					
2	11.5694	9.40707	8.07004	7.21891	6.69044	6.40039
3	18.5742	16.8516	16.6260	16.2824	-105.197	101.583
4	19.9236	18.7853	17.0200	15.9546	15.2702	14.8837
5	5.15918	-19.8390	-24.1967	-24.9607	-25.3434	-25.4942
6	18521.4	16166.9	14541.9	13431.6	12709.3	12301.6
7	402.674	247.290	202.990	180.269	167.354	160.542
8	-120.644	-113.782	-108.362	-104.315	-101.523	-99.8873
9	272.215	3973.65	950.065	182.019	159.915	151.615
10	189.788	167.313	152.549	142.614	136.185	132.562
	$\gamma(-2\omega;\omega,\omega,0)$					
2	58.0764	42.3201	15.3396	9.77463	7.56751	6.59164
3	109.886	68.3358	39.4074	25.7527	-42.3829	-76.5714
4	218.862	34.1920	23.3095	18.4873	16.3995	15.1395
5	-4437.72	-132.706	-16.0488	-9.78176	-24.8011	-25.4004
6	74734.2	33145.2	21761.1	16569.8	13892.9	12571.4
7	-284.225	12612.1	393.905	284.822	189.411	165.016
8	-193.459	-169.226	-126.664	-114.979	-106.029	-100.974
9	-7426.54	2267.11	925.590	163.015	212.338	156.901
10	293.143	420.791	245.073	171.176	146.736	134.959

4. Conclusions

In the present work, density functional theory computations of the nonlinear optical properties of gas-phase gold clusters as a first approach towards the theoretical exploration of their NLO properties are presented. The effects of the incident frequency on the first and second-order hyperpolarizability together with the influence of external electric field on the frontier molecular orbitals of neutral gold clusters are also examined. It is revealed that the application of external electric field may increase or decrease the HOMO-LUMO gap energy of neutral gold clusters depending on the direction and magnitude of the applied field. Moreover, reactive trimer and hexamer gold clusters with small HOMO-LUMO gap energies can be obtained when the external electric field increases in the directions parallel and perpendicular to the molecular plane,

respectively. Furthermore, it is found that the reactivity of a cluster in the presence of external electric field can increase not only due to the decrease in its gap energy, but also because of the change in its geometry, electronic distribution and charge separations. It is predicted that the external electric field has considerable effect on the virtual orbitals of gold hexamer and decreases the energy of these orbitals along the directions parallel to the molecular plane, resulting in the appearance of low-energy excitations that are expected to have important role on the high second-order hyperpolarizability and better response of this cluster to the applied field. The wavelength dispersion plot is also more important for gold hexamer, so that the third-order nonlinear properties of this cluster are strongly affected by the frequency of the incident light and thus can be tuned using the incident frequency for applications.

References

[1] Mirigliano, M., & Milani, P. (2021). Electrical conduction in nanogranular cluster-assembled metallic films. ADV PHYS-X, 6 (1), 1908847.

[2] Song, L., Niedermeier, M. A., Körstgens, V., Löhrer, F. C., Chen, Y., Roth, S. V., & Müller-Buschbaum, P. (2020). In situ study of sputtering nanometer-thick gold films onto 100- nm-thick spiro-OMeTAD Films: implications for perovskite solar cells. ACS Appl. Nano Mater., 3, 5987−5994.

[3] Pečinka, L., Peña-Méndez, E. M., Conde-González, J. E., & Havel, J. (2021). Laser ablation synthesis of metal-doped gold clusters from composites of gold nanoparticles with metal organic frameworks. Sci. Rep., 11, 4656.

[4] Liu, L., & Corma, A. (2020). Evolution of isolated atoms and clusters in catalysis. Trends. Chem., 2 (4), 383-400.

[5] Gao, M., Nakahara, M., Lyalin, A., & Taketsugu, T. (2021). Catalytic activity of gold clusters supported on the h-BN/Au (111) surface for the hydrogen evolution reaction. J. Phys. Chem. C, 125, 1334–1344.

[6] Zhang, X. P., Huang, K. Y., He, S. B., Peng, H. P., Xia, X. H., Chen, W., & Deng, H. H. (2021). Single gold nanocluster probe-based fluorescent sensor array for heavy metal ion discrimination. J. Hazard. Mater., 405, 124259.

[7] Mondal, K., Biswas, S., Singha, T., Chatterjee, U., Datta, P. K., & Kumbhakar, P. (2021). Enhanced optical power limiting and visible luminescence in colloidal dispersion of ultra-small Au nanoclusters synthesized by single-pot chemical technique. J. Mol. Liq., 322, 114909.

[8] Jagannathana, A., Rajaramakrishnaa, R., Rajashekarab, K. M., Gangareddyc, J., Pattar K. V., Rao S. V., Eraiah B., Angadi V. J., Kaewkhaoe, J., & Kothan, S. (2020). Investigations on nonlinear optical properties of gold nanoparticles doped fluoroborate glasses for optical limiting applications. J. Non-Cryst. Solids, 538, 120010.

[9] Sugiuchi, M., Zhang, M., Hakoishi, Y., Shichibu, Y., Horimoto, N. N., Yamauchi, Y., Ishida, Y., & Konishi, K. (2020). Aggregation-mode-dependent optical properties of cationic gold clusters: formation of ordered assemblies in solution and unique optical responses. J. Phys. Chem. C, 124, 16209–16215.

[10] Lou-Franco, J., Das, B., Elliott, C., & Cao, C. (2021). Gold nanozymes: from concept to biomedical applications. Nano-Micro Lett., 13, 10.

[11] Zhang, Y., Li, S., Liu, H., Long, W., & Zhang, X. D. (2020). Enzyme-like properties of gold clusters for biomedical application. Front. Chem., 8, 219.

[12] Zhu, S., Wang, X., Cong, Y., & Li. L. (2020). Regulating the optical properties of gold nanoclusters for biological applications. ACS Omega, 5, 22702−22707.

[13] Bai, X., Wang, Y., Song, Z., Feng, Y., Chen, Y., Zhang, D., & Feng, L. (2020). The basic properties of gold nanoparticles and their applications in tumor diagnosis and treatment. Int. J. Mol. Sci., 21, 2480.

[14] Fan, M., Han, Y., Gao, S., Yan, H., Cao, L., Li, Z., Liang, X. J., & Zhang, J. (2020). Ultrasmall gold nanoparticles in cancer diagnosis and therapy. Theranostics, 10 (11), 4944-4957.

[15] Kim, J., Chun, S. H., Amornkitbamrung, L., Song, C., Yuk, J. S., Ahn, S. Y., Kim, B. W., Lim, Y. T., Oh, B. K., & Um, S. H. (2020). Gold nanoparticle clusters for the investigation of therapeutic efficiency against prostate cancer under near-infrared irradiation. Nano Converg., 7 (1), 5.

[16] Antoine, R., & Bonačić-Koutecký, V. (2018). Liganded silver and gold quantum clusters. Towards a new class of nonlinear optical nanomaterials. SpringerBriefs in Materials, pp 5-27.

[17] Russier-Antoine, I., Bertorelle, F., Vojkovic, M., Rayane, D., Salmon, E., Jonin, C., Dugourd, P., Antoine, R. & Brevet, P. F. (2014). Non-linear optical properties of gold quantum clusters. The smaller the better. Nanoscale, 6, 13572-13577.

[18] Philip, R., Chantharasupawong, P., Qian, H., Jin, R. & Thomas, J. (2012). Evolution of nonlinear optical properties: from gold atomic clusters to plasmonic nanocrystals. Nano Lett., 12, 4661-4667.

[19] Knoppe, S., Häkkinen, H., & Verbiest, T. (2015). Nonlinear optical properties of thiolate-protected gold clusters: a theoretical survey of the first hyperpolarizabilities. J. Phys. Chem. C, 119, 27676-27682.

[20] Knoppe, S., Vanbel, M., Cleuvenbergen, S. V., Vanpraet, L., Bürgi, T., & Verbiest, T. (2015). Nonlinear optical properties of thiolate-protected gold clusters. J. Phys. Chem. C, 119, 6221-6226.

[21] Grobmann, S., Friedrich, D., Karolak, M., Kullock, R., Krauss, E., Emmerling, M., Sangiovanni, G., & Hecht, B. (2019). Nonclassical optical properties of mesoscopic gold. Phys. Rev. Lett., 122, 246802.

[22] Bertorelle, F., Russier-Antoine, I., Calin, N., Comby-Zerbino, C., Bensalah-Ledoux, A., Guy, S., Dugourd, P., Brevet, P. F., Sanader, Ž., Krstić, M., Bonačić-Koutecký, V. & Antoine, R. (2017). $Au_{10}(SG)_{10}$: a chiral gold catenane nanocluster with zero confined electrons. Optical properties and first-principles theoretical analysis. J. Phys. Chem. Lett., 8 (9), 1979-1985.

[23] Barbosa-Silva, R., Silva-Neto, M. L. D., Bain, D., Modesto-Costa, L., Andrade-Fiho, T. S. D., Manzoni, V., Patra, A., & Araujo, C. B. D. (2020). Observation and analysis of incoherent second-harmonic generation in gold nanoclusters with six atoms. J. Phys. Chem. C, 124, 15440–15447.

[24] Hamouda, R., Bellina, B., Bertorelle, F., Compagnon, I., Antoine, R., Broyer, M., Rayane, D., & Dugourd, P. (2010). Electron emission of gas-phase $[Au_{25}(SG)_{18}\text{-}6H]^{7-}$ gold cluster and its action spectroscopy. J. Phys. Chem. Lett., 1, 3189-3194.

[25] Steerteghem, N. V., Clays, K., Verbiest, T., & Cleuvenbergen, S. V. (2017). Third-harmonic scattering for fast and sensitive screening of the second hyperpolarizability in solution. Anal. Chem., 89 (5), 2964-2971.

[26] Bertorelle, F., Moulin, C., Soleihac, A., Comby-Zerbino, C., Dugourd, P., Russier-Antoine, I., Brevet, P. F., & Antoine, R. (2018). Bulky counterions: enhancing the two-photon excited fluorescence of gold nanoclusters. Chem. Phys. Chem., 19 (2), 165-168.

[27] Ramakrishna, G., Varnavski, O., Kim, J., Lee, D., & Goodson, T. (2008). Quantum-sized gold clusters as efficient two-photon absorbers. J. Am. Chem. Soc., 130 (15), 5032-5033.

[28] Iliopoulos, K., Athanasiou, D., Meristoudi, A., Vainos, N., Pispas, S., & Couris, S. (2008). Nonlinear optical properties of Au nanoclusters encapsulated into hybrid block copolymer micelles. Phys. Stat. sol., 205 (11), 2635-2638.

[29] Rojas-Cervellera, V., Rovira, C., & Akola, J. (2015). How do water solvent and glutathione ligands affect the structure and electronic properties of $Au_{25}(SR)_{18}^{-}$. J. Phys. Chem. Lett., 6, 3859–3865.

[30] Gürdal, E., Horneber, A., Shaqqura, N., Meixner, A. J., Kern, D. P., Zhang, D., & Fleischer, M. (2020). Enhancement of the second harmonic signal of nonlinear crystals by self-assembled gold nanoparticles. J. Chem. Phys., 152, 104711.

[31] Gomes, A. S. L., Maldonado, M., Menezes, L. D. S., Acioli, L. H., Araújo, C. B. D., Dysart, J., Doyle, D., Johns, P., Naciri, J., Charipar, N., & Fontana, J. (2020). Linear and third-order nanlinear optical properties of self-assembled plasmonic gold metasurfaces. Nanophotonics 9 (4), 725-740.

[32] Rout, A., Boltaev, G. S., Ganeev, R. A., Fu, Y., Maurya, S. K., Kim, V. V., Rao, K. S., & Guo, C. (2019). Nonlinear optical studies of gold nanoparticle films. Nanomaterials, 9, 291.

[33] Panoiu, N. C., Sha, W. E. I., Lei, D. Y., & Li, G. C. (2018). Nonlinear optics in plasmonic nanostructures. J. Opt., 20, 083001.

[34] Gruene, P., Butschke, B., Lyon, J. T., Rayner, D. M., & Fielicke, A. (2014). Far-IR spectra of small neutral gold clusters in the gas phase. Z. Phys. Chem., 228 (4-5), 337-350.

[35] Loginova, A. S., Savintseva, L. A., & Ignatov, S. K. (2019). Structure and electronic excitation spectra of low-lying isomers of Au_n clusters (n=2-20). A DFT study. Computational and Theoretical Chemistry, 1170, 112637.

[36] Walker, A. V. (2005). Structure and energetics of small gold nanoclusters and their positive ions. J. Chem. Phys., 122, 094310.

[37] Zanti, G., & Peeters, D. (2013). Electronic structure analysis of small gold clusters Au_m ($m \leq 16$) by density functional theory. Theor. Chem. Acc., 132, 1300.

[38] Assadollahzadeh, B., & Schwerdtfeger, P. (2009). A systematic search for minimum structures of small gold clusters Aun (n=2–20) and their electronic properties. J. Chem. Phys., 131, 064306.

[39] Singh, N. B., & Sarkar, U. (2015). Geometry, chemical reactivity and Raman spectra of gold clusters. Cogent Chem., 1, 1076713.

[40] Pyykkö, P. (2004). Theoretical chemistry of gold. Angew. Chem. Int. Ed., 43, 4412-4456.

[41] Hay, P. J., & Wadt, W. R. (1985). Ab initio effective core potentials for molecular calculations. Potentials for K to Au including the outermost core orbitals. J. Chem. Phys., 82 (1), 299-310.

[42] Hay, P. J., & Wadt, W. R. (1985). Ab initio effective core potentials for molecular calculations. Potentials for the transition metal atoms Sc to Hg. J. Chem. Phys., 82 (1), 270-283.

[43] Wadt, W. R., & Hay, P. J. (1985). Ab initio effective core potentials for molecular calculations. Potentials for main group elements Na to Bi. J. Chem. Phys., 82, 284-298.

[44] Cowan, R. D., & Griffin, D. C. (1976). Approximate relativistic corrections to atomic radial wave functions. J. Opt. Soc. Am., 66 (10), 1010-1014.

[45] Schwerdtfeger, P., & Nagle, J. K. (2019). 2018 Table of static dipole polarizabilities of the neutral elements in the periodic table. Mol. Phys., 117 (9-12), 1200-1225.

[46] Likura, H., Tsuneda, T., Yanai, T., & Hirao, K. (2001). A long-range correction scheme for generalized-gradient-approximation exchange functionals. J. Chem. Phys., 115, 3540-3544.

[47] Piela, L. (2007). Ideas of Quantum Chemistry. 1st ed., Elsevier B. V., pp 615-647.

[48] Kdikara, M. S., Stranger, R., & Humphrey, M. G. (2018). Computational studies of the nonlinear optical properties of organometallic complexes. Coord. Chem. Rev., 375, 389-409.

[49] Tarazkar, M., Romanov, D. A., & Levis, R. J. (2015). Theoretical study of second-order hyperpolarizability for nitrogen radical cation. J. Phys. B: At. Mol. Opt. Phys., 48 (9), 094019.

[50] Rice, J. E. (1990). Frequency dependent hyperpolarizabilities with application to formaldehyde and methyl fluoride. J. Chem. Phys., 93, 8828.

[51] Frisch, M. J., Trucks, G. W., Schlegel, H. B., Scuseria, G. E., Robb, M. A., Cheeseman, J. R., Scalmani, G., Barone, V., Mennucci, B., Petersson, G. A., Nakatsuji, H., Caricato, M., Li, X., Hratchian, H. P., Izmaylov, A. F., Bloino, J., Zheng, G., Sonnenberg, J. L., Hada, M., Ehara, M., Toyota, K., Fukuda, R., Hasegawa, J., Ishida, M., Nakajima, T., Honda, Y., Kitao, O., Nakai, H., Vreven, T., Montgomery, J. A., Jr., Peralta, J. E., Ogliaro, F., Bearpark, M., Heyd, J. J., Brothers, E., Kudin, K. N., Staroverov, V. N., Kobayashi, R., Normand, J., Raghavachari, K., Rendell, A., Burant, J. C., Iyengar, S. S., Tomasi, J., Cossi, M., Rega, N., Millam, J. M., Klene, M., Knox, J. E., Cross, J. B., Bakken, V., Adamo, C., Jaramillo, J., Gomperts, R., Stratmann, R. E., Yazyev, O., Austin, A. J., Cammi, R., Pomelli, C., Ochterski, J. W., Martin, R. L., Morokuma, K., Zakrzewski, V. G., Voth, G. A., Salvador, P., Dannenberg, J. J., Dapprich, S., Daniels, A. D., Farkas, O., Foresman, J. B., Ortiz, J. V., Cioslowski, J. & Fox, D. J. Gaussian 09, Gaussian, Inc., Wallingford, Revision D. 01 (2013).

[52] Denninngton, R. D., Keith, T. A., & Millam, J. M. GaussView 5.0.8, 2000-2008.

[53] O´Boyle, N. M., Tenderholt, A. L., & Langner, K. M. (2008). A library for package‐independent computational chemistry algorithms. J. Comp. Chem., 29, 839-845.

[54] Glendening, E. D., Reed, A. E., Carpenter, J. E., & Weinhold. F., NBO Version 3.

[55] Choi, Y. C., Pak, C., & Kim, K. S. (2006). Electric field effects on water clusters (n=3-5): systematic ab initio study of structures, energetics and transition states. J. Chem. Phys., 124, 094308.

[56] Stuyver, T., Danovich, D., Joy, J., & Shaik, S. (2019). External electric field effects on chemical structure and reactivity. WIREs Comput. Mol. Sci., 10 (2), e1438.

[57] Chanana, G., Batra, K., & Prasad, V. (2019). Exploring response of Li_2 molecule to external electric field: a DFT and SAC-CI study. Computational and Theoretical Chemistry, 1169, 112620.

[58] Wang, J., Yang, M., Wang, G., & Zhao, J. (2003). Dipole polarizabilities of germanium clusters. Chem. Phys. Lett., 367 (3-4), 448–454.

[59] Janjua, M. R. S. A., Mahmood, A., Nazar, M. F., Yang, Z., & Pan, S. (2014). Electronic absorption spectra and nonlinear optical properties of Ruthenium acetylide complexes: a DFT study toward the designing of new high NLO response compounds. Acta Chim. Slov., 61, 382-390.

[60] Janjua, M. R. S. A. (2018). Structural properties and nonlinear optical responses of halogenated compounds: a DFT investigation on molecular modelling. Open Chem., 16, 978-985.

[61] Li, H., Xu, H., Shen, X., Han, K., Bi, Z., & Xu, R. (2016). Size-, electric-field-, and frequency-dependent third-order nonlinear optical properties of hydrogenated silicon nanoclusters. Scientific Reports, 6, 28067.